symmetry

MDPI

*Article*

# Coplanar Waveguide (CPW) Loaded with Symmetric Circular and Polygonal Split-Ring Resonator (SRR) Shapes

**Supakorn Harnsoongnoen [1,*], Saksun Srisai [1] and Pongsathorn Kongkeaw [2]**

[1] The Biomimicry for Sustainable Agriculture, Health, Environment and Energy Research Unit, Department of Physics, Faculty of Science, Mahasarakham University, Kantarawichai District, Maha Sarakham 44150, Thailand; 64010262001@msu.ac.th

[2] Program of Physics, Faculty of Science and Technology, Rajabhat Maha Sarakham University, Muang Maha Sarakham District, Maha Sarakham 44000, Thailand; pongsathorn.ko@rmu.ac.th

* Correspondence: supakorn.h@msu.ac.th

**Abstract:** This paper investigates the performance of coplanar waveguide (CPW) structures loaded with symmetric circular and polygonal split-ring resonators (SRRs) for microwave and RF applications, leveraging their unique electromagnetic properties. These properties make them suitable for metamaterials, sensors, filters, resonators, antennas, and communication systems. The objectives of this study are to analyze the impact of different SRR shapes on the transmission characteristics of CPWs and to explore their potential for realizing compact and efficient microwave components. The CPW-SRR structures are fabricated on a dielectric substrate, and their transmission properties and spectrogram are experimentally characterized in the frequency range of 4 GHz to 10 GHz with the rotation angles of the SRR gap. The simulation results demonstrate that the resonant frequencies and magnitude of the transmission coefficient of the CPW-SRR structures are influenced by the geometry of the SRR shapes and the rotation angles of the SRR gap, with certain shapes exhibiting enhanced performance characteristics compared to others. Moreover, the symmetric circular and polygonal SRRs offer design flexibility and enable the realization of miniaturized microwave components with improved performance metrics. Overall, this study provides valuable insights into the design and optimization of CPW-based microwave circuits utilizing symmetric SRR shapes, paving the way for advancements in the miniaturization and integration of RF systems.

**Keywords:** coplanar waveguide (CPW); split-ring resonators (SRRs); microwave sensors; polygonal shapes; spectrogram

check for updates

**Citation:** Harnsoongnoen, S.; Srisai, S.; Kongkeaw, P. Coplanar Waveguide (CPW) Loaded with Symmetric Circular and Polygonal Split-Ring Resonator (SRR) Shapes. *Symmetry* **2024**, *16*, 534. https://doi.org/10.3390/sym16050534

Academic Editor: Theodore E. Simos

Received: 25 March 2024
Revised: 23 April 2024
Accepted: 24 April 2024
Published: 29 April 2024



## 1. Introduction

Versatile structures known as split-ring resonators (SRRs) have emerged as remarkable entities, showcasing promising potential across a broad spectrum of operating frequencies spanning from microwave (MW) to the optical regime. Initially proposed on theoretical grounds in 1996 by Pendry et al. [1], the concept of SRRs gained tangible realization with the successful fabrication of an SRR in 2000 by Smith et al. [2], followed by the pivotal experimental verification of a negative index of refraction in 2001 by Shelby et al. [3]. SRRs have further been integrated with planar transmission lines, facilitating the synthesis of transmission line metamaterials. Notably, Martin et al. [4] in 2003 and Falcone et al. [5] in 2004 demonstrated that coupling SRRs with coplanar waveguides (CPWs) on the back substrate side effectively inhibits signal propagation in the vicinity of SRR resonance. This coupling mechanism underscores the versatility and practical implications of SRRs in manipulating electromagnetic waves across various frequencies and applications. The introduced novel compact electromagnetic bandgap (EBG) structures using complementary split-ring resonators (CSRRs) was proposed by Falcone et al. (2004) [6]. Baena et al. (2005) expanded the field by presenting analytical models for isolated and coupled SRRs/CSRRs, thus paving the way for the design of compact microwave devices based on metamaterial concepts [7]. Subsequent researchers, starting with Naqui et al. in 2011, have explored the diverse applications of SRRs and CSRRs, particularly in sensor technologies [8]. These resonators exhibit the ability to suppress both odd and even modes in CPWs [9]. Experimental validation supports selective mode suppression in CPWs. Notably, Naqui et al. further analyzed the significance of symmetric resonators in CPWs, highlighting their role in enabling unhindered signal propagation and the detection of asymmetry with notable sensitivity [10]. Expanding on these findings, researchers proposed microwave sensors utilizing the symmetry properties of transmission lines, ensuring robustness against environmental changes and material variations [11]. Additionally, investigations into CPWs loaded with electric-LC (ELC) resonators for sensor applications, including angular displacement and velocity measurements, were put forth with a focus on robust design principles [12]. Further innovations were introduced, including angular displacement and velocity sensors employing S-shaped split-ring resonators (S-SRRs) [13] and a golden spiral-shaped tapered ring resonator [14] for enhanced dynamic range. Additionally, compact filters utilizing CPWs loaded with S-shaped split-ring resonators were proposed, with a validated lumped-element circuit model supported by electromagnetic simulations [15]. The exploration of CPW-based microwave components continued with the introduction of broadband microstrip filters using open complementary split-ring resonators (OCSRRs) [16]. Demonstrated designs included displacement sensors and dual-mode bandpass filters, showcasing the potential of resonator configurations in practical applications [17]. A novel dual-band filter design incorporating microstrip stepped impedance resonator (MSIR) and defected stepped impedance resonator (DSIR) filters was proposed [18]. Dual-frequency printed dipoles with SRRs were developed to maintain dipolar radiation patterns, consequently improving antenna efficiency [19]. Advancements were not limited to antennas; proposals for multiband printed monopole antennas and chipless RFID systems based on resonators were put forth [20–23].

The narrative of CPW-loaded resonator structures unfolds with a series of innovative strides propelled by intensive studies on sensor technologies [24]. These investigations have primarily focused on alignment detection, linear displacement measurement, and rotational sensing, thereby showcasing substantial enhancements in linearity and dynamic range [25–27]. Notably, these advancements have underpinned the evolution of CPW resonator structures, with recent endeavors exemplifying their utility in the real-time monitoring of various concentrations through the integration of CPWs with SRRs [28–30]. This integration has unveiled promising prospects for their application in biochemical sensing domains. Furthermore, the exploration has expanded to encompass novel designs, such as metamaterial-inspired microwave microfluidic sensors, illustrating the adaptability and versatility of resonator-based technologies across diverse scientific and engineering disciplines [31,32]. The realm of resonator applications traverses a broad spectrum of challenges, ranging from leveraging symmetric split-ring resonators (SRRs) to excite asymmetric resonance for specialized tasks like narrowband filtering and bio-sensors [33] to employing a single-ring square resonator (S-SRR) in conjunction with multiple double-split square ring resonators (D-SRRs) for permittivity characterization [34]. Innovations extend to novel methodologies such as integrating a split-ring metasurface-loaded honeycomb sandwich structure, which serves as an effective solution to counteract the stealth performance degradation of aircraft with substantial curvature [35]. Moreover, the development of a compact and highly sensitive microwave sensor, employing a complementary split-ring resonator (CSRR) for liquid characterization, underscores the practical versatility of resonator-based technologies [36]. Additionally, the implementation of a microwave dual-crack sensor, harnessing the $TE_{20}$ resonance of a CSRR on a substrate-integrated waveguide (SIW), highlights the potential of resonators in sensing applications [37]. These diverse applications underscore the far-reaching impact and multifaceted utility of resonator technologies across various fields of study and practical domains. In light of these advancements, concerted efforts have been directed towards establishing comprehensive guidelines for the design of resonator-based devices, with a particular emphasis on harnessing resonator symmetry to enhance device efficiency across diverse applications [38–42]. Recently, there have been presentations on the applications of CPW structures loaded with SRRs for MEMS [43,44], the detection of dielectric constants [45], and barcode applications [46]. However, amidst these significant strides, a notable research gap arises regarding the performance characterization of coplanar waveguides (CPWs) with an SRR gap rotation angle spanning from 0° to 90°. Intriguingly, this aspect remains largely unexplored and necessitates thorough scrutiny and analysis. Thus, we are propelled by an intrinsic motivation to embark upon a pioneering investigation aimed at shedding light on this uncharted territory.

Our study endeavors to undertake a meticulous examination of the influence exerted by diverse SRR shapes on the transmission characteristics and spectrogram of CPWs. By meticulously dissecting this phenomenon, we aspire to unravel novel insights poised to facilitate the realization of compact and highly efficient microwave components. This exploration not only contributes to the advancement of the frontiers of microwave engineering but also underscores the intrinsic flexibility and adaptability inherent within CPW-loaded resonator structures, thereby catalyzing further innovations in this burgeoning field.

## 2. Materials and Methods

### *2.1. CPW-Loaded SRR Structures*

Figure 1 illustrates the configurations of coplanar waveguide (CPW)-loaded split-ring resonator (SRR) structures. The array encompasses nine distinct SRR geometries, namely circular, triangular, quadrilateral, pentagonal, hexagonal, heptagonal, octagonal, nonagonal, and decagonal. The design process employs a DiClad880 substrate characterized by a dielectric constant ($\varepsilon_r$) of 2.2 and a loss tangent (tan $\delta$) of 0.0009, with a substrate thickness of 1.6 mm. The detailed layout schematics and dimensional specifications of the CPW-loaded SRR structures are presented in Table 1.

**Table 1.** Geometrical parameters of a CPW loaded with symmetric circular and polygonal SRR shapes.

| Parameter | W | W_GND | L | c | g | r | s |
|---|---|---|---|---|---|---|---|
| Value (mm) | 4.95 | 14.85 | 60.4 | 0.5 | 0.3 | 6 | 0.3 |

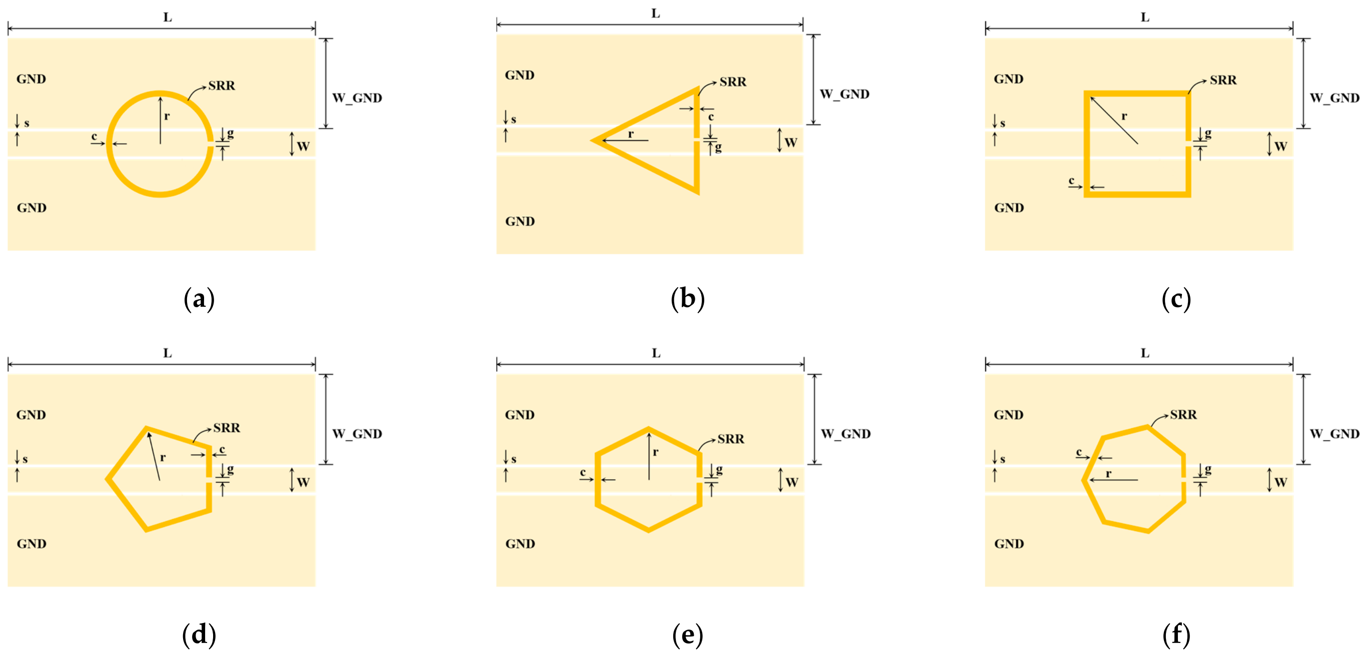


**Figure 1.** *Cont.*

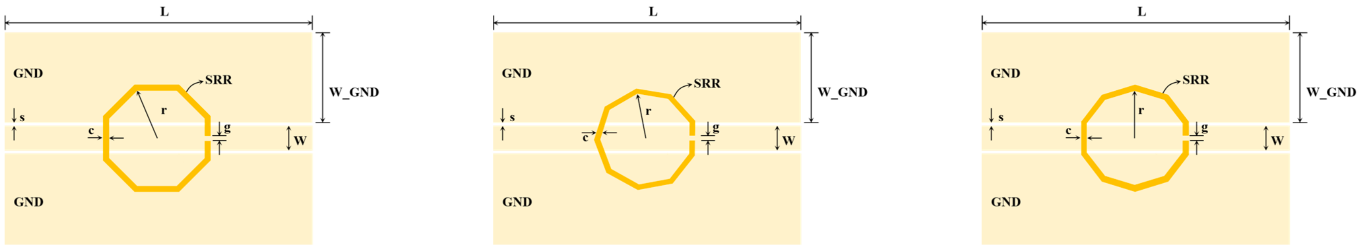


(**g**) (**h**) (**i**)

**Figure 1.** The proposed CPW SSRRs: (**a**) circular, (**b**) triangular, (**c**) quadrilateral, (**d**) pentagonal, (**e**) hexagonal, (**f**) heptagonal, (**g**) octagonal, (**h**) nonagonal, and (**i**) decagonal.

### *2.2. Equivalent Circuit Model*

The elucidation of the equivalent circuit model concerning the CPW loaded with an SRR is presented in Figure 2. This model is intertwined with the theoretical underpinnings of CPWs loaded with symmetric resonators. Within this construct, the designations $L_1$ and $L_2$ outline the metallic transmission line. Additionally, $C_1$ serves as a pivotal component, characterizing the coupling capacitance linking the metallic transmission line with the metallic ground. Notably, the interplay between the metallic transmission line and ground with the SRR is elucidated through the comprehensive representation of capacitances denoted by $C_2$, $C_3$, $C_4$, and $C_5$. The sum of $C_1$ to $C_5$ can be represented as $C_M$. Moreover, the SRR finds its essence within the realm of the equivalent circuit models, epitomized by the designations $L_{SRR}$ and $C_{SRR}$. The resonance frequency ($F_r$), manifested by the notch magnitude in the transmission coefficient, can be expressed as follows:

$$F_r = \frac{1}{2\pi\sqrt{L_{SRR}(C_{SRR} + C_M)}} \tag{1}$$

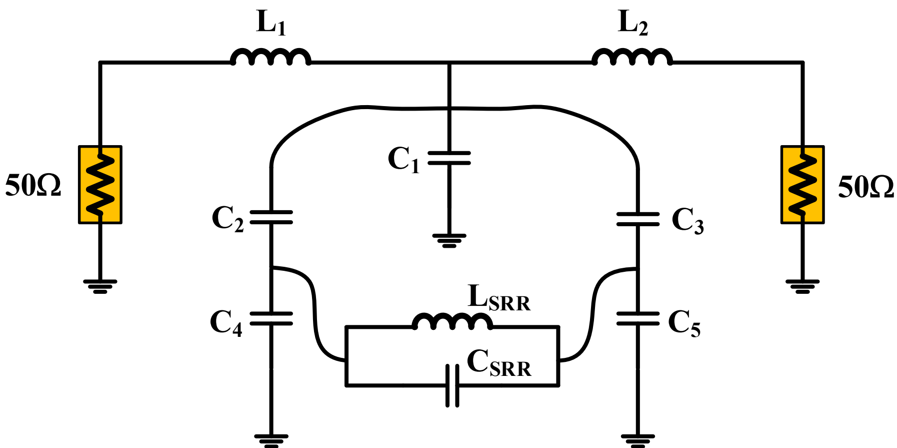


**Figure 2.** Equivalent circuit model of CPW loaded with SRR.

### *2.3. Transmission Coefficient and Resonance Frequency for CPW-Loaded SRR Structures in Free Space with Rotation Angles of Gap Ranging from 0° to 90°*

CPW-loaded SRR structures encompass a diverse array of nine distinct configurations, namely circular, triangular, quadrilateral, pentagonal, hexagonal, heptagonal, octagonal, nonagonal, and decagonal. Each SRR structure features a gap, with the rotation angles of said gap spanning from 0° to 90° in increments of 10°. To comprehensively characterize the performance of these structures, a frequency sweep is conducted within the range of 4 GHz to 10 GHz, utilizing 2001 sampling points. The resonance frequencies and magnitude of transmission coefficients for the nine SRRs, accounting for gap orientations ranging from 0° to 90°, are meticulously recorded and subjected to thorough analysis. This exhaustive examination aims to elucidate the intricate interplay between SRR geometry, gap orientation, and microwave transmission characteristics, thereby contributing to a deeper understanding of the underlying principles governing CPW-loaded resonator behavior.

### 2.4. The Spectrogram of CPW-Loaded SRRs

The spectrogram provides a comprehensive visualization of the spectra of transmission coefficients across a range of gap rotation angles, spanning from $0^\circ$ to $180^\circ$ in increments of $10^\circ$. To construct the spectrogram, the collected transmission coefficient spectra are meticulously analyzed, with the transmission coefficients plotted as a function of both frequency and angle position. This graphical representation facilitates the identification of resonance frequencies and the examination of how these resonances vary with changes in gap orientation. By scrutinizing the spectrogram, valuable insights can be gleaned regarding the influence of gap rotation angles on the transmission characteristics of CPW-loaded SRR structures. The positioning of the SRR gap influences the coupling capacitance of the CPW loaded with an SRR, thereby altering the resonance frequency. Furthermore, the resulting symmetry of the system impacts the magnitude of the transmission coefficient. This analytical approach serves to deepen our understanding of the intricate interplay between structural parameters and microwave transmission properties, thereby contributing to the advancement of CPW-based microwave component design and optimization.

### 2.5. Fabrication and Experimental Measurement Set-Up

The CPW loaded with the SRR was fabricated via the dry film photoresist lithography technique, and it was bonded with an SMA connector. The CPW loaded with the SRR with the gap at $0^\circ$ and $90^\circ$ is as illustrated in Figure 3a,b, respectively. The device was connected to a vector network analyzer (Agilent E5071B vector) through a high-frequency (HF) coaxial cable, as depicted in Figure 3c. The connection between the device and the coaxial cable was established using an SMA connector interfaced with the vector network analyzer (VNA).

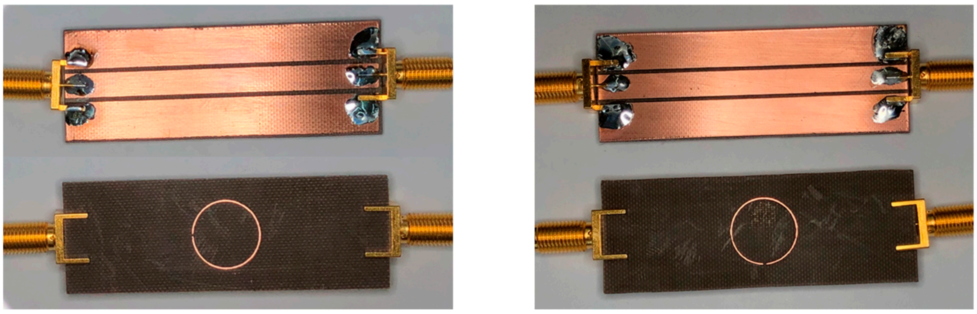

(**a**) (**b**)

**Figure 3.** *Cont.*

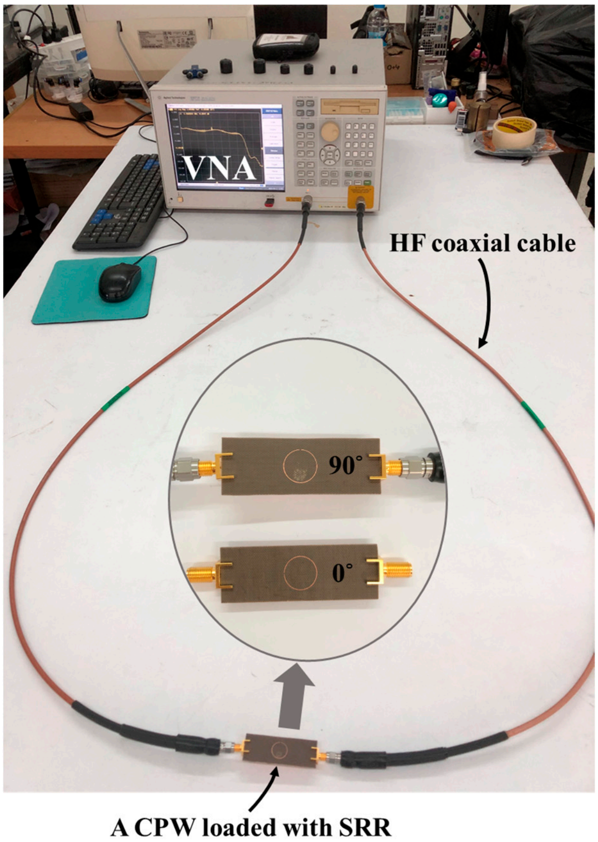


(**c**)

**Figure 3.** Device prototype (W = 4.95 mm, W_GND = 13.23 mm, L = 60.40 mm, c = 0.3 mm, g = 0.3 mm, r = 6 mm, and s = 0.5 mm) and measurement set-up. (**a**) CPW loaded with SRR with gap at θ = 0°, (**b**) CPW loaded with SRR with gap at θ = 90°, and (**c**) measurement set-up.

## 3. Results

### *3.1. Transmission Coefficient for CPW-Loaded SRR Structures with Gap at θ = 0° and θ = 90°*

Figure 4 provides a detailed examination of the $S_{21}$ spectra for CPW-loaded split-ring resonator (SRR) structures in free space, presenting data for the rotation angles of the gap at θ = 0° and θ = 90°. Figure 4a,b offer three-dimensional renderings of the structures, while Figure 4c,d present them in two dimensions. The analysis of the simulation results reveals distinct trends in resonance frequency ($F_r$) as a function of gap rotation angle and SRR shape. Notably, it is observed that the resonance frequency at θ = 0° is consistently lower than that at θ = 90° across all SRR shapes. Furthermore, among the various SRR geometries, the circular SRR consistently exhibits the lowest $F_r$, while the triangular SRR consistently displays the highest $F_r$ values, irrespective of gap orientation. Intriguingly, the $F_r$ values exhibit a discernible trend across the different SRR shapes, with a consistent ranking from low to high $F_r$ observed across both θ = 0° and θ = 90° configurations. Specifically, the $F_r$ values ascend in the following order: circular, decagonal, nonagonal, octagonal, heptagonal, hexagonal, pentagonal, quadrilateral, and triangular SRRs. These findings shed light on the nuanced interplay between SRR geometry, gap orientation, and resonance frequency, thereby enriching our understanding of the underlying mechanisms governing the microwave transmission characteristics of CPW-loaded resonator structures. Such insights hold significant implications for the design and optimization of compact and efficient microwave components tailored to specific application requirements.

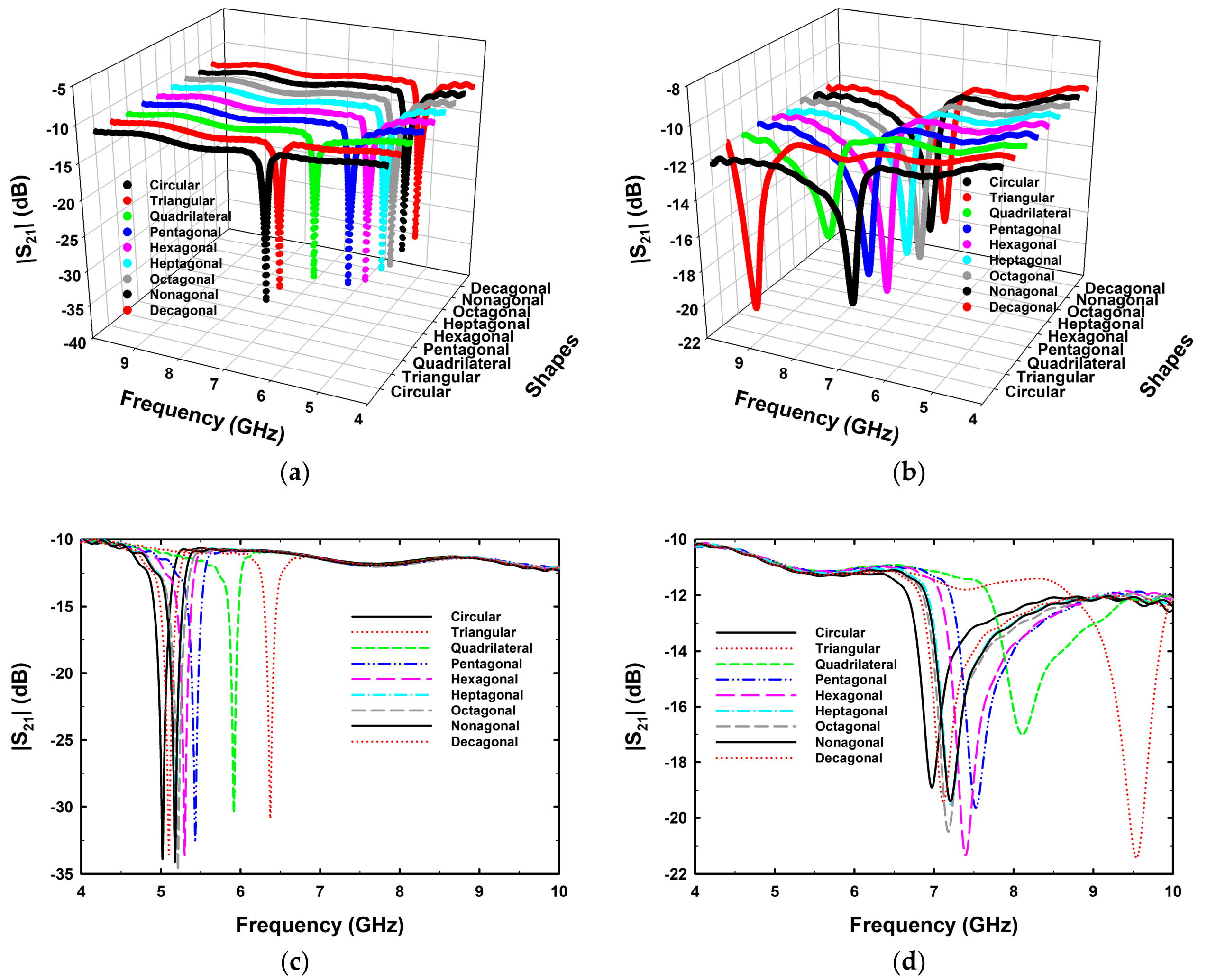


**Figure 4.** The $S_{21}$ spectra of CPW SSRRs with the rotation angle of the gap at (**a**) θ = 0° in 3D, (**b**) θ = 90° in 3D, (**c**) θ = 0° in 2D, and (**d**) θ = 90° in 2D.

Figure 5 presents the outcomes of a rigorous linear regression analysis aimed at elucidating the relationship between the number of angles (*NOA*) characterizing polygonal split-ring resonator (SRR) shapes and their corresponding $S_{21}$ values. The analysis harnesses a comprehensive dataset comprising diverse polygonal SRR shapes, each associated with a distinct *NOA*, alongside their measured $S_{21}$ values obtained under controlled experimental conditions. The linear regression analysis is conducted employing the least squares method, endeavoring to establish the optimal-fitting line that captures the relationship between the predictor variable (the number of angles) and the response variable ($S_{21}$). The regression line depicted in the graph serves as the best linear approximation of this relationship. The formulation of the regression line is expressed by the following equations:

$$S_{21} = -0.2007 \times NOA - 31.8885 \quad (2)$$

$$S_{21} = -0.0564 \times NOA - 19.3638 \quad (3)$$

Equation (2), with the rotation angle of the gap set at 0°, yields a coefficient of determination ($R^2$) for the regression model of 0.19. This $R^2$ value signifies that approximately 19% of the variation observed in $S_{21}$ can be elucidated by the number of angles characterizing polygonal SRR shapes. Consequently, a weak linear relationship between the two variables is inferred. Conversely, Equation (3), corresponding to a rotation angle of the gap at 90°, generates an $R^2$ for the regression model of 0.02. This $R^2$ value indicates that merely 2% of the observed variation in $S_{21}$ can be attributed to the number of angles of polygonal SRR shapes, implying an exceedingly weak linear relationship between these variables. The dashed line incorporated into the graph signifies the 95% confidence intervals. In statistical analysis, confidence intervals provide a range within which it can be reasonably inferred that the true value of a parameter resides. Notably, from Equations (2) and (3), when considering the 95% confidence intervals, the quadrilateral SRR structure exhibits the lowest confidence interval for $S_{21}$. This meticulous statistical examination provides invaluable insights into the relationship between polygonal SRR shapes' geometric characteristics and their microwave transmission properties. Such insights are instrumental in informing the design and optimization of CPW-loaded resonator structures, paving the way for the development of highly efficient and tailored microwave components.

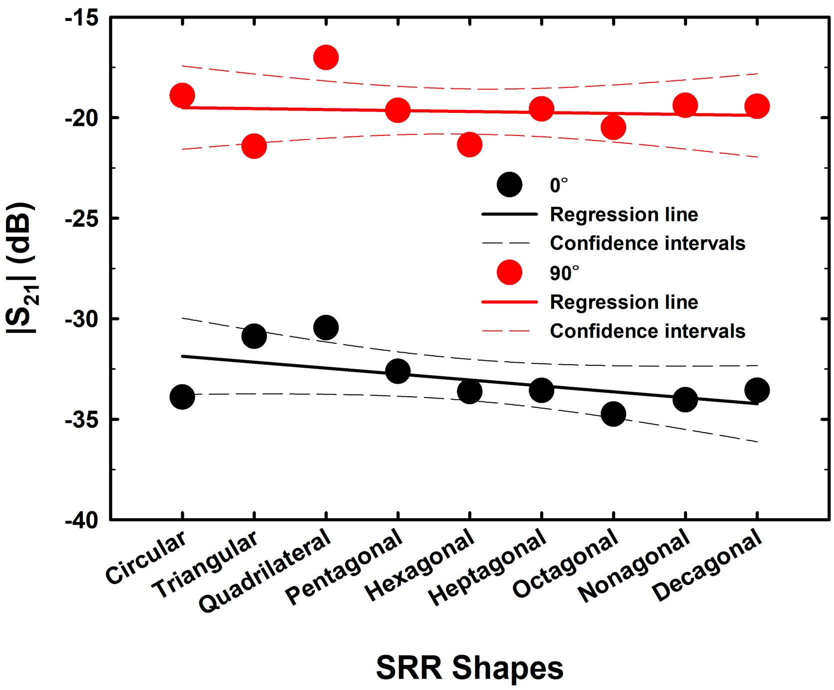


**Figure 5.** The correlation between $S_{21}$ and circular and polygonal SRR shapes with the rotation angle of the gap at 0° and 90°.

Figure 6a visually represents the correlation between resonance frequency ($F_r$) and polygonal split-ring resonator (SRR) shapes, taking into account rotation angles of the gap set at 0° and 90°. A further exploration of this relationship is provided in Figure 6b,c, which delve into the correlation between $F_r$ and the number of angles characterizing polygonal SRR shapes, ranging from three to ten angles, in conjunction with the rotation angle of the gap set at 0° and 90°. To quantitatively analyze this relationship, Equations (4) and (5) are formulated:

$$F_r = 5.1001 + 7.6229 \times e^{-0.5895 \times NOA} \quad (4)$$

$$F_r = 7.1644 + 36.2381 \times e^{-0.9083 \times NOA} \quad (5)$$

Here, *NOA* denotes the number of angles in the polygonal SRR shapes. The regression analysis yields a high $R^2$ of 0.9852 and 0.9978 for Equations (4) and (5), respectively, signifying a strong correlation between $F_r$ and the geometric parameters characterizing SRR shapes. The simulation results presented in Figure 6a–c intricately explore the intricate relationship between $F_r$ and various configurations of polygonal SRR structures. In Figure 6a, it is observed that the value of $F_r$ at a 90° rotation angle surpasses that at a 0° rotation angle. This analysis offers valuable insights into the variations in $F_r$ concerning different shapes and orientations of SRR structures. Figure 6b,c provide a more detailed examination by investigating the correlation between $F_r$ and the number of angles in polygonal SRR shapes. Spanning from three to ten angles, this range offers a comprehensive perspective on how the geometric complexity of SRR shapes influences $F_r$. Notably, this investigation also considers the rotation angle of the gap at 0° and 90°, thereby underscoring the significance of orientation in the observed trends. The empirical findings are further elucidated through Equations (4) and (5), which quantitatively characterize the relationship between $F_r$ and the geometric parameters of SRR shapes. The elevated $R^2$ values affirm the robustness of the proposed equations in capturing this relationship. Overall, it is apparent that the relationship between the number of angles of the SRR and $F_r$, with gaps at the 0° and 90° angle positions, is governed by the same exponential decay function. Additionally, the analysis reveals that the 0° angle position yields a lower $F_r$, with the circular structure consistently exhibiting the lowest $F_r$ in both the 0° and 90° cases.

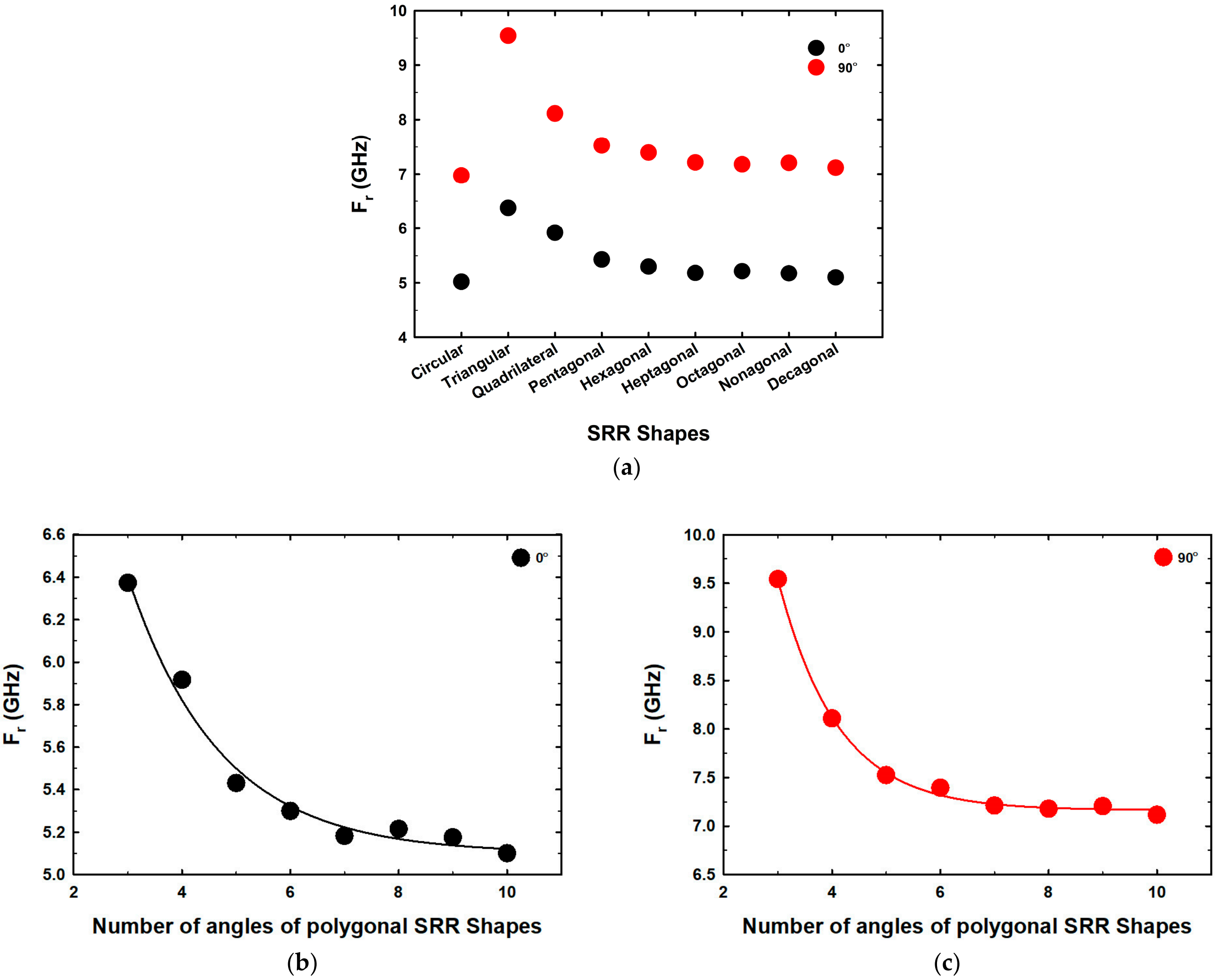


**Figure 6.** The correlation between $F_r$ and (**a**) polygonal SRR shapes with the rotation angle of the gap at 0° and 90°; the correlation between $F_r$ and the number of angles of polygonal SRR shapes ranging from three to ten angles, also in relation to the rotation angle of the gap at (**b**) 0° and (**c**) 90°.

*3.2. Transmission Coefficient for CPW-Loaded SRR Structures with Rotation Angles for Gap Ranging from 0° to 90°*

Figure 7 visually portrays the configurations of coplanar waveguide (CPW)-loaded split-ring resonator (SRR) structures, showcasing a comprehensive range of rotation angles for the gap spanning from 0° to 90°. Each subfigure from Figure 7a–i provides a detailed depiction of the respective structures, encompassing circular, triangular, quadrilateral, pentagonal, hexagonal, heptagonal, octagonal, nonagonal, and decagonal SRR shapes, respectively. In Figure 7a, the circular SRR structure is depicted, characterized by its symmetrical and continuous circular geometry. This configuration serves as a fundamental building block in SRR-based microwave components due to its simplicity and uniformity. Subsequent subfigures, from Figure 7b–i, progressively introduce polygonal SRR shapes with increasing numbers of edges, resulting in geometric variations that influence microwave transmission characteristics. The triangular SRR depicted in Figure 7b introduces a degree of angular complexity compared to the circular counterpart, contributing to altered resonance behavior and enhanced versatility in microwave applications. As the polygonal SRR shapes become more intricate, such as the quadrilateral, pentagonal, and hexagonal shape and beyond, Figure 7 provides a visual representation of how the geometric complexity impacts the structural and electromagnetic properties of CPW-loaded SRR configurations. Each subfigure in Figure 7 offers valuable insights into the geometric intricacies and structural variations inherent to CPW-loaded SRR structures, highlighting the diverse design possibilities and the potential for tailored microwave component optimization. These visual representations serve as a foundational resource for further exploration and analysis, facilitating a deeper understanding of the interplay between geometry, gap rotation angles, and microwave transmission characteristics in CPW-based resonator systems.

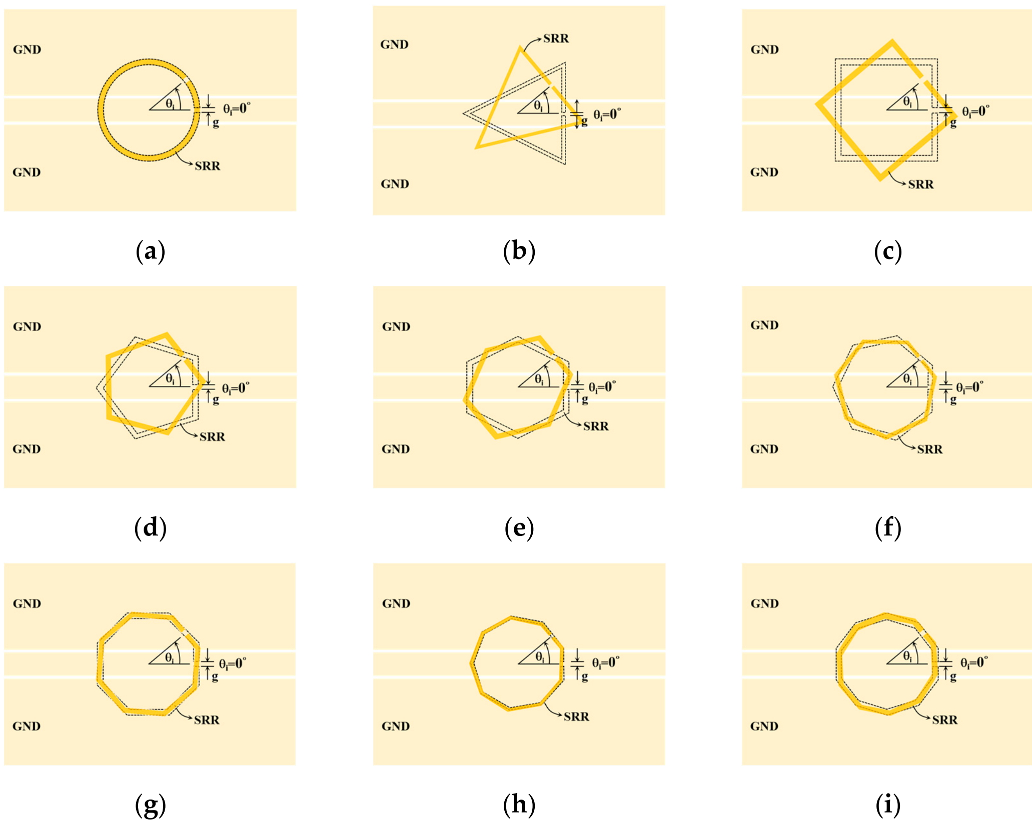


**Figure 7.** The CPW-loaded SRRs with rotation angles for the gap ranging from 0° to 90°, featuring the following shapes: (**a**) circular, (**b**) triangular, (**c**) quadrilateral, (**d**) pentagonal, (**e**) hexagonal, (**f**) heptagonal, (**g**) octagonal, (**h**) nonagonal, and (**i**) decagonal.

Figure 8 presents the $S_{21}$ spectra for coplanar waveguide (CPW)-loaded split-ring resonator (SRR) structures in free space, showcasing a range of rotation angles for the gap varying from 0° to 90°. Each subfigure from Figure 8a–i offers a detailed representation of the corresponding SRR structure, encompassing circular, triangular, quadrilateral, pentagonal, hexagonal, heptagonal, octagonal, nonagonal, and decagonal shapes, respectively. Observing the $S_{21}$ spectra within the frequency range of 4 to 10 GHz, considering the rotation angle of the gap spanning from 0° to 90°, reveals two distinct characteristics of $F_r$ peaks. Notably, these characteristics manifest in instances of both single and double peaks, indicating the presence of varied resonance behavior across different SRR configurations and gap orientations. The spectral analysis depicted in Figure 8 provides valuable insights into the microwave transmission characteristics of CPW-loaded SRR structures, shedding light on the nuanced interplay between geometric parameters, gap rotation angles, and resonance phenomena. Each subfigure offers a comprehensive view of the structural and electromagnetic properties inherent to different polygonal SRR shapes, contributing to a deeper understanding of the design considerations and optimization strategies for CPW-based microwave components. These spectral observations underscore the importance of meticulous analysis and characterization in elucidating the complex behavior of SRR-based microwave devices. Furthermore, they serve as a foundation for further investigation into the optimization of CPW-loaded resonator structures for diverse applications in microwave engineering.

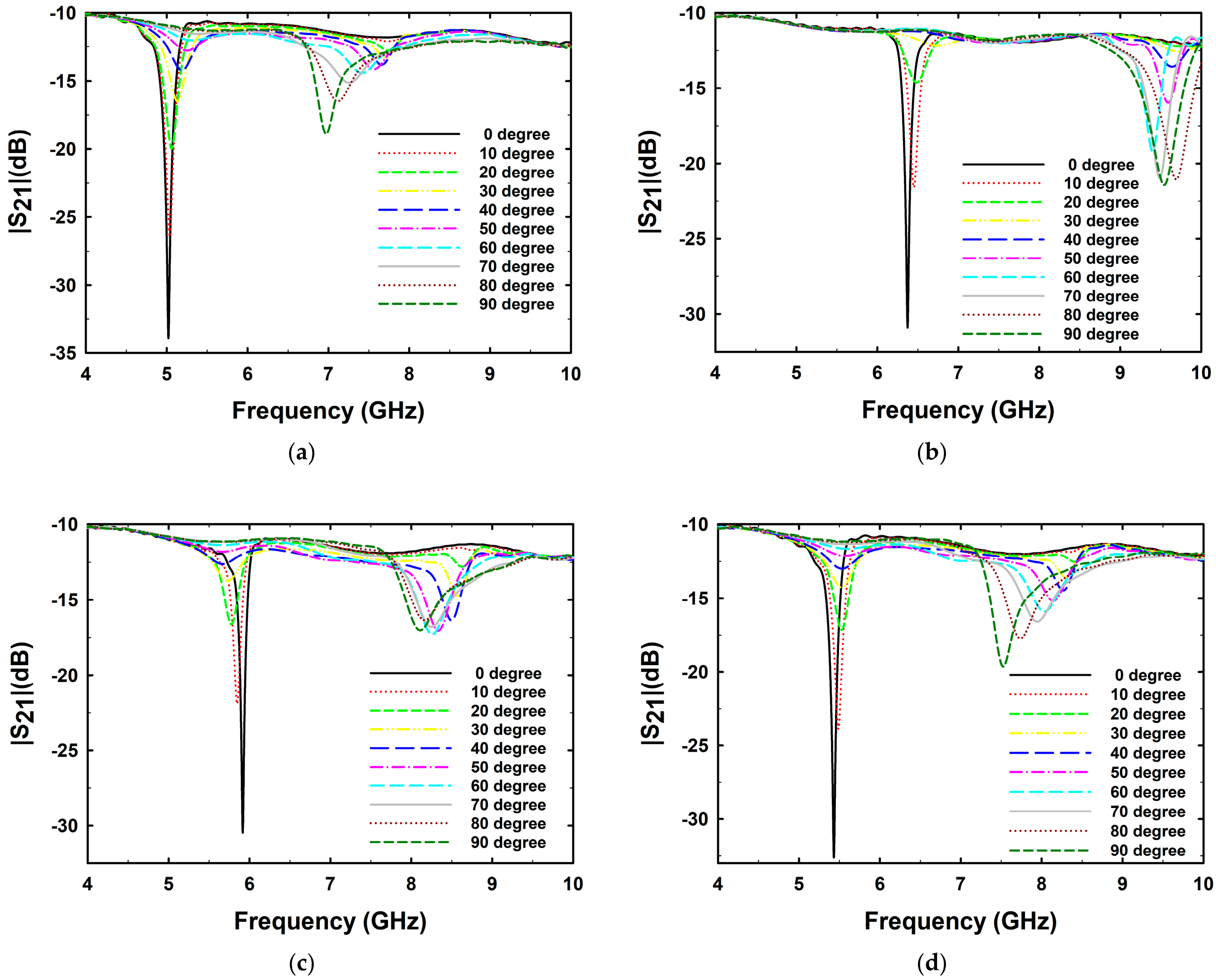


**Figure 8.** *Cont.*

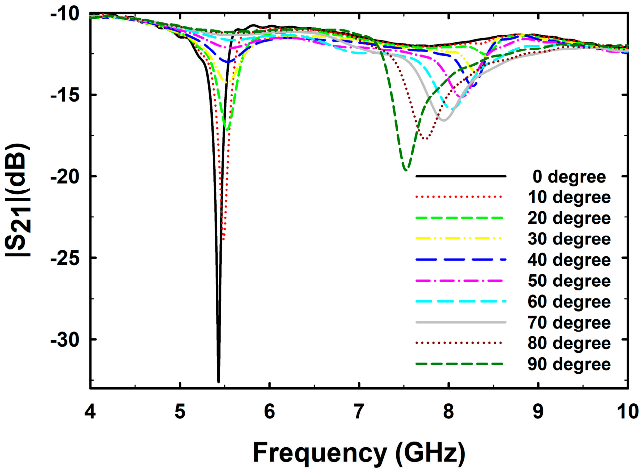


(**e**)

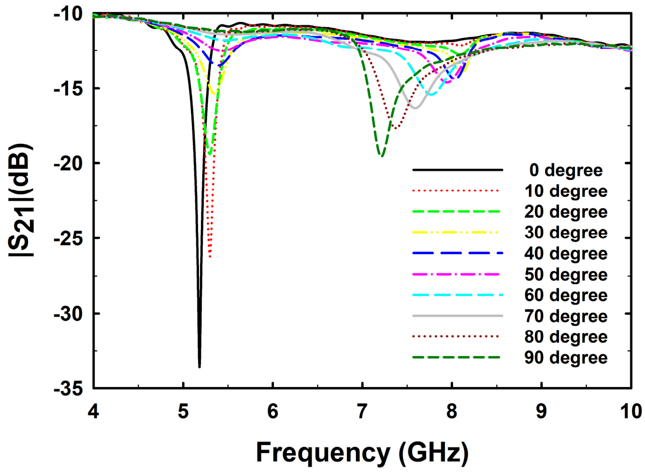


(**f**)

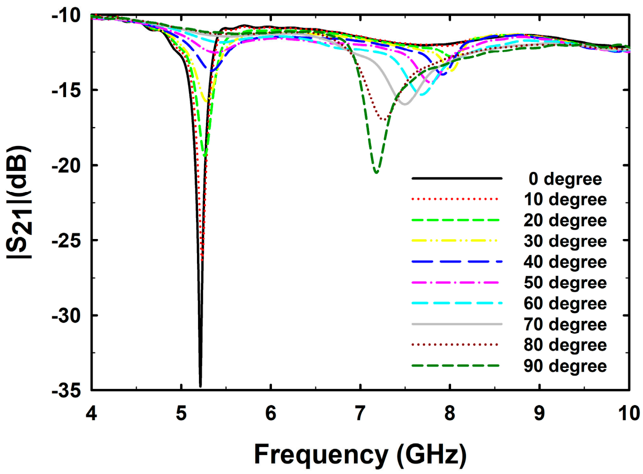


(**g**)

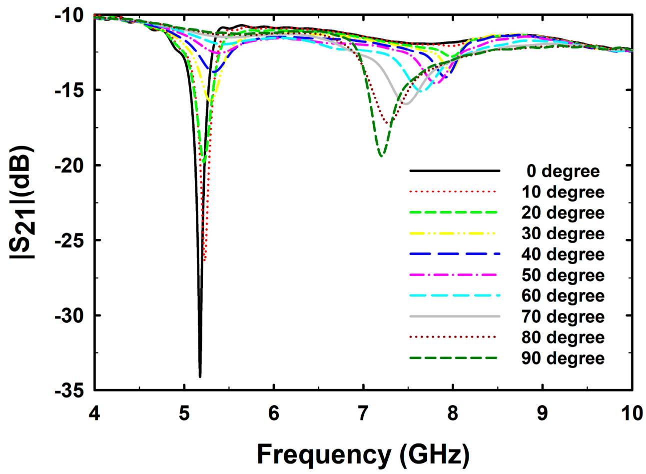


(**h**)

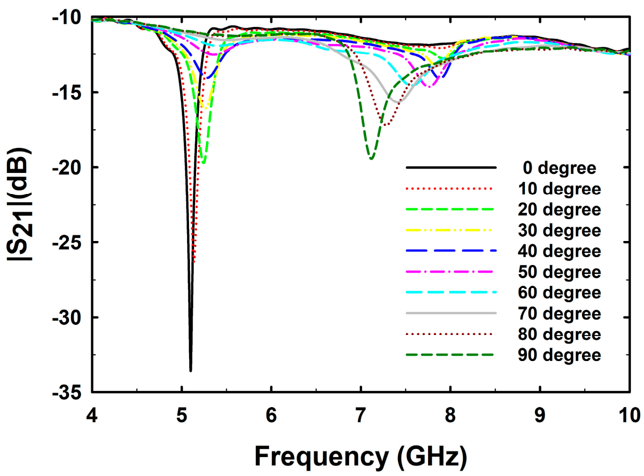


(**i**)

**Figure 8.** The $S_{21}$ spectra of CPW-loaded SRRs: (**a**) circular, (**b**) triangular, (**c**) quadrilateral, (**d**) pentagonal, (**e**) hexagonal, (**f**) heptagonal, (**g**) octagonal, (**h**) nonagonal, and (**i**) decagonal.

The analysis of the $S_{21}$ spectra reveals distinct patterns in resonance behavior corresponding to rotation angles of the gap in coplanar waveguide (CPW)-loaded split-ring resonator (SRR) structures. Notably, it was observed that a single $F_r$ peak emerges during specific convolution periods, ranging from 0° to 20°and from 80° to 90°. The initial single peak manifests within the convolution period spanning from 0° to 20°, while the second single peak arises within the rotation range of 80° to 90°. Conversely, between the gap angles of 30° and 70°, two peaks are evident, indicating a more complex resonance behavior within this range. Figure 9 illustrates the correlation between $S_{21}$ values at rotation angles of 0° and all other rotation angles for the gap of CPW-loaded SRRs while varying the frequency from 4 GHz to 10 GHz. Specifically, Figure 9a depicts the correlation between the $S_{21}$ values of circular SRRs from 0° to 90°, while Figure 9b shows the correlation between the $S_{21}$ values of circular SRRs from 100° to 180°. Notably, cyclic patterns are observed between 0° and 90°, suggesting a symmetrical response in $S_{21}$ values across this rotation angle range. The observed cyclic patterns in the correlation between $S_{21}$ values and rotation angles of the gap in CPW-loaded SRR structures imply the presence of inherent symmetrical characteristics. This symmetry is particularly pronounced within the range spanning from 0° to 90°, indicating a consistent and predictable behavior in microwave transmission properties for polygonal SRR shapes coupled with coplanar waveguides. These findings contribute to a deeper understanding of the structural and electromagnetic characteristics of CPW-loaded SRR configurations, highlighting the importance of symmetry considerations in microwave component design and optimization. Such insights are crucial for the development of highly efficient and tailored microwave devices with enhanced performance and functionality.

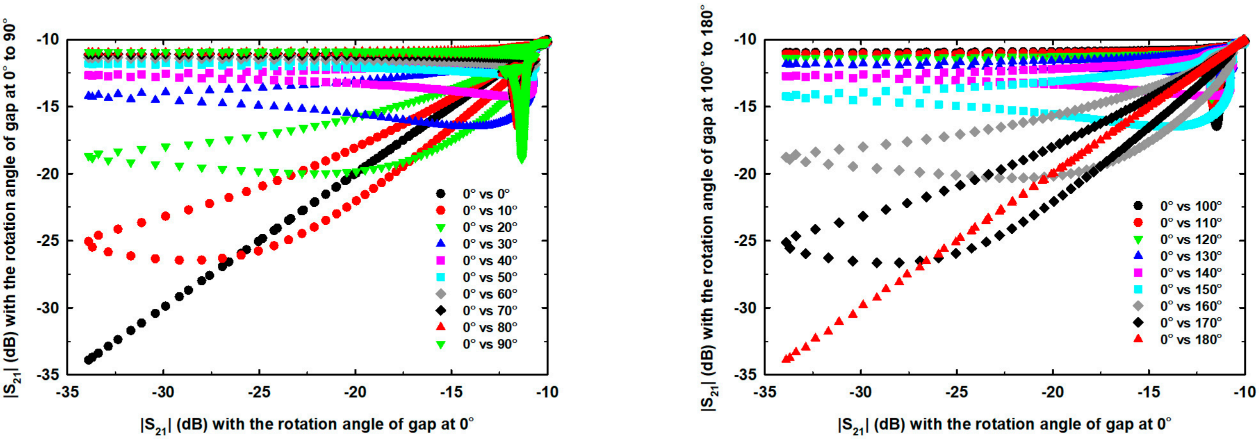


(**a**) (**b**)

**Figure 9.** The correlation between the $S_{21}$ values at the rotation angles of 0° and all rotation angles for the gap of CPW-loaded SRRs when varying the frequency from 4 GHz to 10 GHz, a (**a**) circular SRR (0° to 90°) and (**b**) circular SRR (100° to 180°).

Figure 10 presents a comprehensive analysis of the intricate relationship between the $S_{21}$ magnitude, representing the highest amplitude, and resonance frequency ($F_r$) values, with respect to the rotation angles of the split-ring resonator (SRR) gap ranging from 0° to 90°. This examination is conducted while modulating the frequency between 4 GHz and 10 GHz, providing a detailed insight into the dynamic behavior of CPW-loaded SRR structures under varying geometric configurations. The graphical representation in Figure 8 unveils a compelling correlation, demonstrating that changes in the angles of the SRR gap induce corresponding shifts in $S_{21}$ across all structures under investigation. Notably, a rapid and pronounced alteration in magnitude is observed within the initial 0° to 30° span, followed by a subsequent decrement. This consistent pattern of variation persists across all examined structures, depicting a coherent trend amidst diverse structural configurations. Moreover, a nuanced examination of the plotted data reveals intriguing fluctuations within the triangular and quadrilateral SRR structures, particularly evident between 30° and 90°, as delineated in Figure 10a. This observation underscores the sensitivity of these structures to variations in gap angles, elucidating the subtle nuances inherent in their performance characteristics across varying geometric configurations. Delving deeper into the analysis, an exploration of $F_r$ variation concerning the gap position of the SRR within the 0° to 90° ambit uncovers the presence of two distinct $F_r$ ranges within each structural configuration. Noteworthy is the discernible fluctuation in $F_r$ levels within the narrower angle range of 20° to 40°, suggestive of localized perturbations in the electromagnetic response of the structures under scrutiny. Overall, the findings presented in Figure 10 provide valuable insights into the complex interplay between geometric parameters, resonance behavior, and microwave transmission properties in CPW-loaded SRR structures. This comprehensive analysis enhances our understanding of the underlying mechanisms governing the performance of these structures and lays the groundwork for future advancements in microwave component design and optimization.

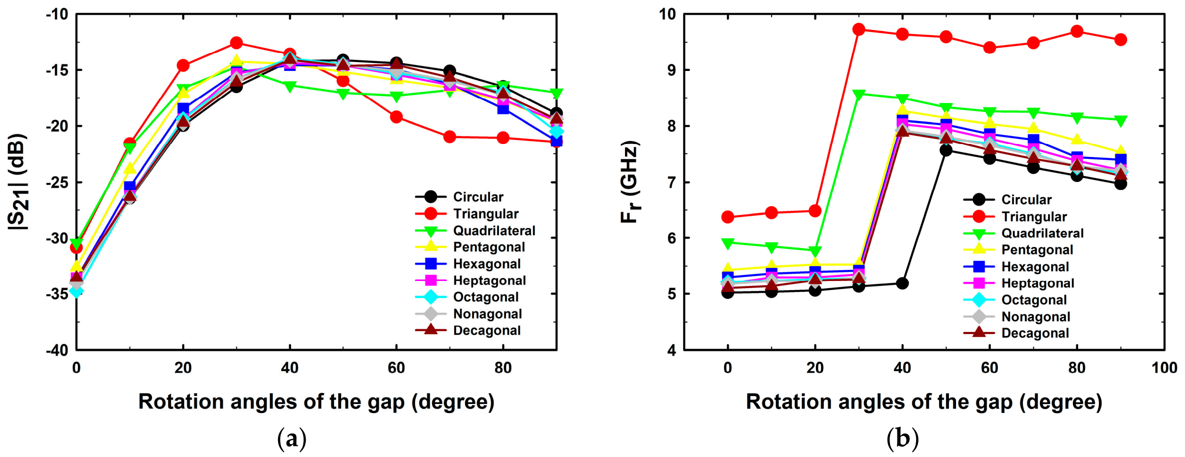


**Figure 10.** The correlation between the $S_{21}$ and $F_r$ values with the rotation angles of the gap at 0° to 90° when varying the frequency from 4 GHz to 10 GHz, (**a**) $S_{21}$ and (**b**) $F_r$.

Moreover, a comparative evaluation across the range of angles reveals intriguing disparities in resonance frequency ($F_r$) values among different split-ring resonator (SRR) geometries. Notably, the triangular SRR structure emerges as the frontrunner in $F_r$ magnitude, exhibiting heightened sensitivity to gap angle variations. This is because the triangular SRR structure is small, with the least amount of copper area. As a result, the triangular SRR structure's capacitor and the coupling capacitor have less coupling. This results in a higher $F_r$ compared to other structures. Moreover, the triangular SRR structure has sharp corners and a high electric field distribution. This indicates a higher sensitivity than other structures. In contrast, the circular SRR structure consistently occupies the opposite end of the spectrum, displaying the lowest $F_r$ values across the entire 0° to 90° spectrum, as illustrated in Figure 10b. However, we found that octagonal, nonagonal, and decagonal structures have similar spectral responses, with $S_{21}$ and $F_r$ values varying in a very similar way with the gap rotation angle. This is because the three structures have similar sizes and copper areas. This stark contrast underscores the pivotal role of structural geometry in dictating electromagnetic response characteristics, offering valuable insights into the design and optimization of SRR-based devices across a diverse array of applications. The observed variations in $F_r$ values highlight the intricate interplay between SRR geometry, gap angle, and microwave transmission properties, emphasizing the importance of a tailored structural design in achieving desired performance outcomes. These findings contribute to a deeper understanding of the complex behavior of CPW-loaded SRR structures and provide crucial guidance for optimizing their performance in various microwave engineering applications. By elucidating the influence of structural geometry on $F_r$ values, this comparative assessment facilitates informed decision-making in the design and development of SRR-based devices, ultimately leading to enhanced efficiency and functionality in microwave systems.

Figure 11 shows the electric field distribution on the top layer of CPW-loaded SRRs with symmetrical circular and polygonal SRR shapes at gap positions at 0°. Upon observing the electric field distribution, it was discovered that the CPW loaded with a triangular SRR exhibited the highest electric field distribution value when the gap was at 0°. This is because the structure features sharp corners and is constrained within its confines.

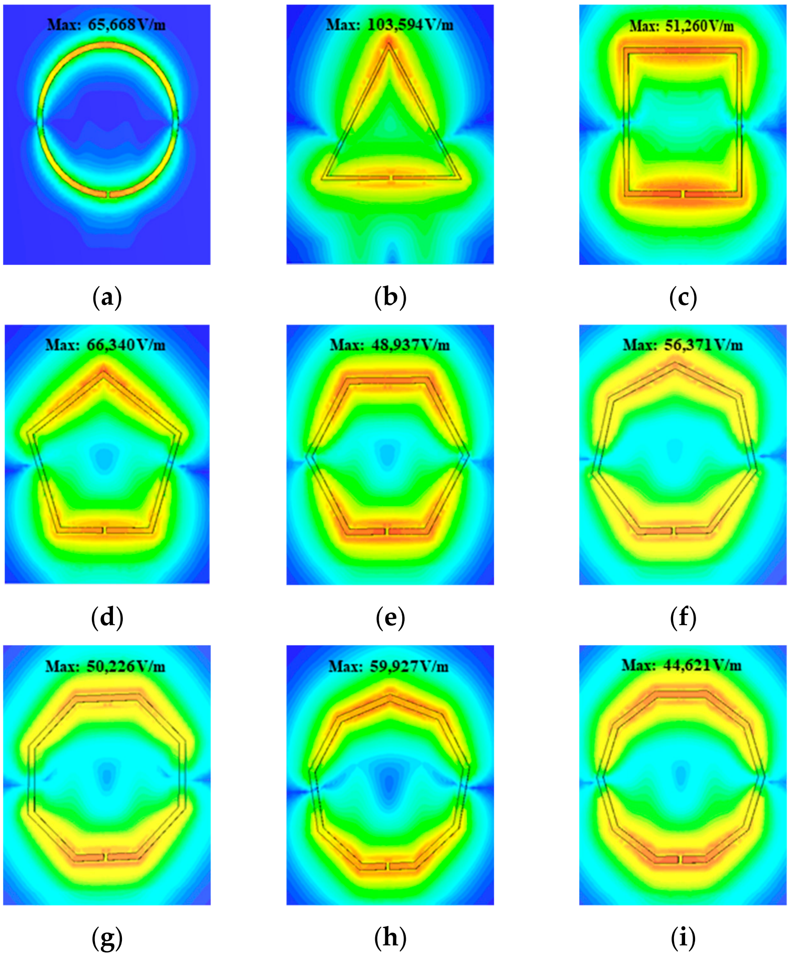


**Figure 11.** The electric field distribution on the top layer of CPW-loaded SRRs within the gap rotation angle at 0°: (**a**) circular, (**b**) triangular, (**c**) quadrilateral, (**d**) pentagonal, (**e**) hexagonal, (**f**) heptagonal, (**g**) octagonal, (**h**) nonagonal, and (**i**) decagonal.

Furthermore, we have discovered that the coplanar waveguide (CPW) loaded with a split-ring resonator (SRR) structure yields a more robust electric field compared to the microstrip loaded with an SRR structure. The enhanced electric field renders the region highly sensitive, making it suitable for sensor applications. Hence, we have opted to investigate the CPW structure loaded with an SRR in this study. Nevertheless, our investigation revealed that the microstrip structure loaded with a triangle SRR exhibits an exceptionally high electric field in comparison to all other structures. Additionally, it also entails an elevated resonant frequency when compared to the CPW loaded with a triangle SRR. These yielded inverse results compared to microstrips loaded with other SRRs. This is likely because the triangle SRR structure is small and possesses sharp corners. This involves positioning the copper area of the structure as close to and covering the microstrip area as possible. Figure 12 displays the spectra of $S_{21}$. Simulation and measurement tend to agree; the position of the gap at 0°, the $F_r$, is lower than that at 90°. We have found that the measurement results have shifted from the simulation, influenced by fluctuations stemming from fabrication and variations in the size of the structure at different points during the etching process in copper. The proposed structure is capable of generating a high electric field, rendering it suitable for highly sensitive sensing applications across solid, liquid, and gaseous states. Additionally, its responsiveness to changes in both position and angle qualifies it for measuring various parameters such as displacement, rotation, angular displacement, velocity, alignment, and position. Simultaneously, featuring a two-port design and demonstrating signal propagation inhibition near the resonant frequency of the SRR, the structure presents an alternative avenue for utilization as a microwave frequency filter circuit.

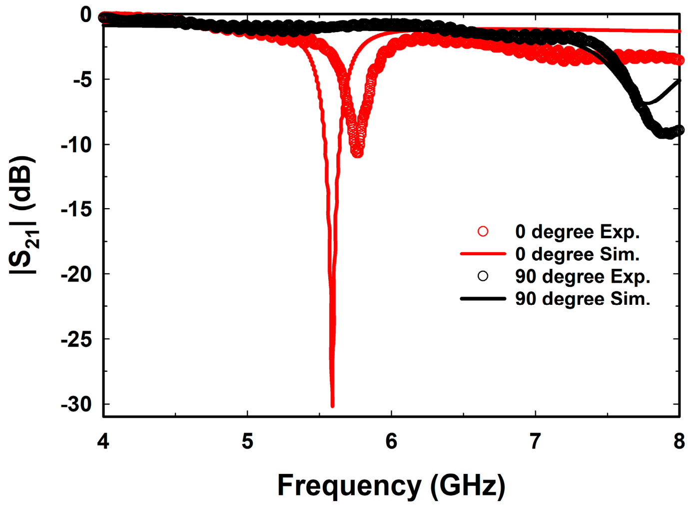


**Figure 12.** $S_{21}$ spectra of CPW loaded with SRR with gap at θ = 0° and θ = 90° based on simulation (Sim.) and experiment (Exp.), W = 4.95 mm, W_GND = 13.225 mm, L = 60.40 mm, c = 0.3 mm, g = 0.3 mm, r = 6 mm, and s = 0.5 mm.

Figure 13 shows the spectrogram of a coplanar waveguide (CPW) loaded with symmetrical circular and polygonal split-ring resonator (SRR) shapes at gap positions at various rotation angles. This visual representation offers insights into the transmission coefficient spectra across gap rotation angles ranging from 0° to 180° at 10° intervals. By synthesizing these transmission coefficient spectra, a comprehensive spectrogram emerges, plotting transmission coefficients as a function of both frequency and angle position. In this spectrogram, the contrast between the red and blue hues is indicative: the red regions denote areas with minimal $S_{21}$ magnitude, while the blue regions signify pronounced $S_{21}$ magnitudes. This observation is pivotal, as it delineates the areas where resonant frequencies manifest. Notably, alterations in the gap angle prompt discernible shifts in both $S_{21}$ and the resonant frequency ($F_r$), as evidenced across Figure 13a–i. Upon closer examination, the blue region, symbolizing the resonant frequency zone, can be delineated into three distinct segments: the first spanning from 0° to 20°, the second from 80° to 100°, and the third from 160° to 180°. Remarkably, the angle intervals of 0° to 20° and 80° to 100° coincide within the same frequency range, albeit featuring varying $F_r$ values across each structural configuration. Moreover, upon scrutinizing the spectrogram of each individual structure, a notable symmetry emerges within the gap rotation angle ranges of 0° to 90° and 91° to 180°. This observation underscores the inherent balance and coherence in the structural arrangements across these specific angular domains. The presence of such symmetry highlights the predictable and consistent behavior exhibited by CPW-loaded SRR structures under varying gap rotation angles, underscoring their potential for robust and reliable performance across diverse applications in microwave engineering. Based on the spectrograms depicted in Figure 13, it can be concluded that all nine SRR-loaded CPW structures exhibit symmetry within the angle range of 0° to 90°. Additionally, the magnitude of $S_{21}$ and the resonant frequency differ for each position of the gap.

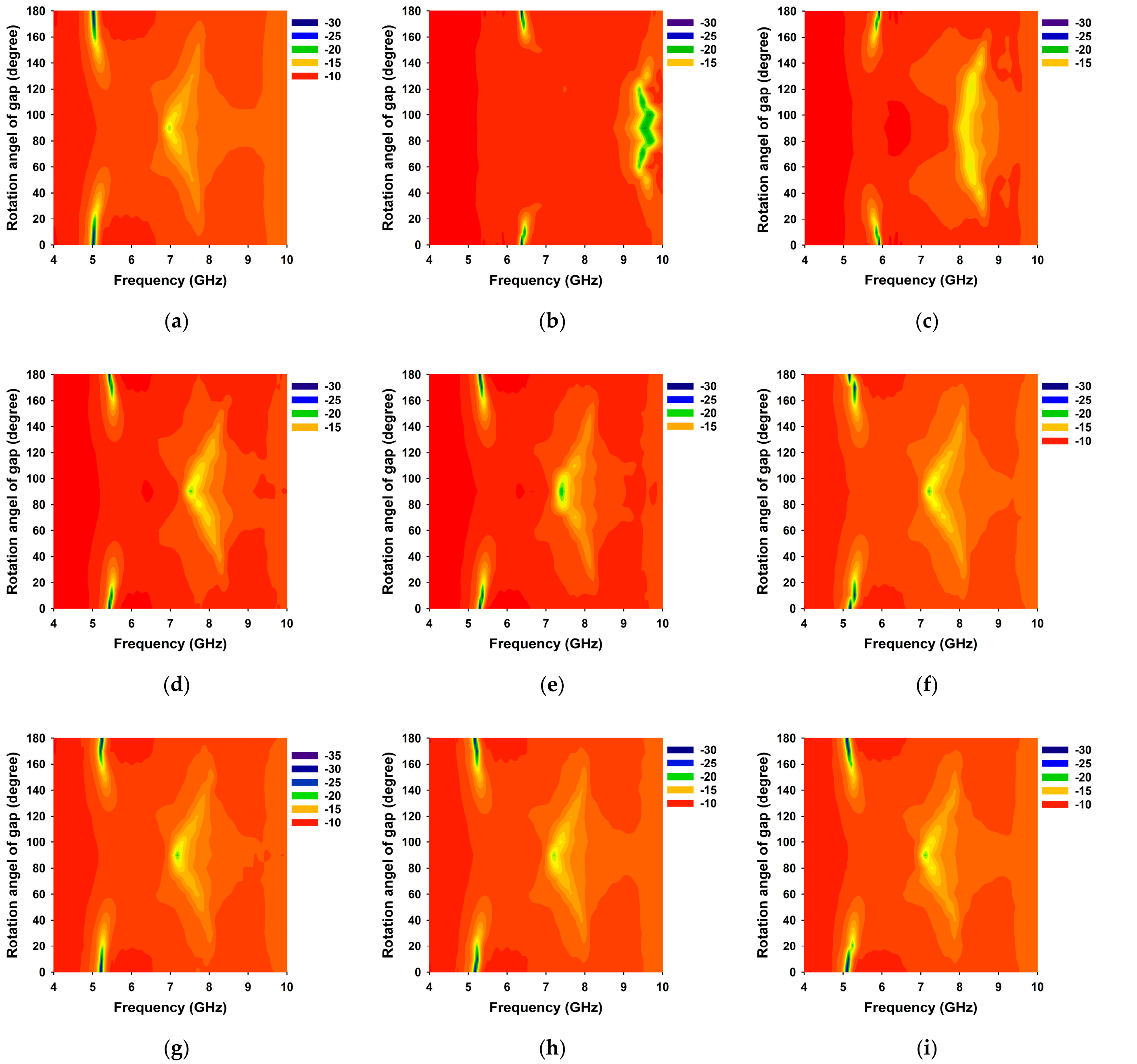


**Figure 13.** The spectrogram of CPW-loaded SRRs: (**a**) circular, (**b**) triangular, (**c**) quadrilateral, (**d**) pentagonal, (**e**) hexagonal, (**f**) heptagonal, (**g**) octagonal, (**h**) nonagonal, and (**i**) decagonal.

The sensitivity ($S$) of the rotation angles of the gap from 0° to 90° was analyzed from the results shown in Figure 14. The sensitivity was defined as the ratio of the resonant frequency change to the angles of the gap change, as follows:

$$S = \frac{\Delta F_r}{\Delta \theta} \tag{6}$$

where $\Delta F_r$ is the shift in the resonant frequency ($F_{r\_\theta} - F_{r\_0^\circ}$), and $\Delta\theta$ is the change in the angles of the gap ($\theta - 0^\circ$). From Figure 14, it is shown that the sensitivity of every structure is divided into two ranges. The sensitivity is ordered from the highest to lowest as follows: triangle (0.47 GHz/degree), quadrilateral (0.36 GHz/degree), pentagon (0.33 GHz/degree), hexagon

(0.31 GHz/degree), heptagon (0.30 GHz/degree), octagon (0.29 GHz/degree), nonagon (0.29 GHz/degree), decagon (0.29 GHz/degree), and circle (0.25 GHz/degree), respectively.

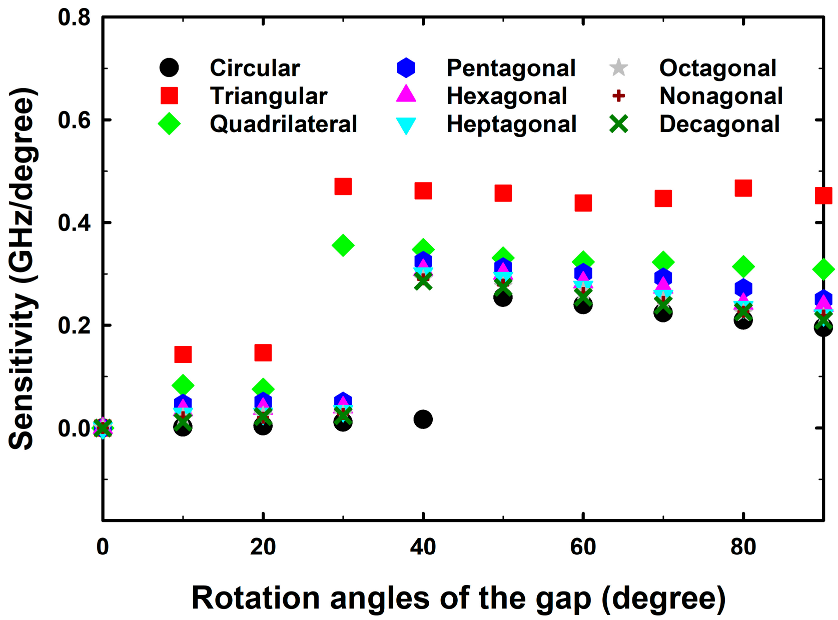


**Figure 14.** A sensitivity comparison of the CPW-loaded SRRs for rotation angles of the gap at 0° to 90°.

Comparisons of the performance of a CPW loaded with symmetric circular and polygonal SRR shapes are shown in Table 2. It was found that the structure with the lowest $F_r$ was the CPW loaded with circular SRRs, while the structure with the smallest size of SRRs and the least copper area of SRRs was the CPW loaded with triangular SRRs. Additionally, it was observed that the CPW loaded with triangular SRRs also provides the highest electric field distribution value. It was further noted that structures with an odd number of corners position their corners exactly in the center of the transmission line and provide a higher electric field distribution than structures with an even number of corners. Moreover, the sharper the angle, the higher the electric field distribution value will be.

**Table 2.** Comparisons of the performance of a CPW loaded with symmetric circular and polygonal SRR shapes.

| SRR Shapes | Sum of Internal Angles (Degrees) | Radius (mm) | Circumference Length (mm) | Area ($m^2$) | Copper Area ($m^2$) | $\lvert S_{21} \rvert$ (dB) | $F_r$ (GHz) | E-Field (V/m) | S (GHz/ Degree) |
|---|---|---|---|---|---|---|---|---|---|
| Circular | 0 | 6 | 37.70 | 113.10 | 19.63 | −33.90 | 5.02 | 65,668 | 0.25 |
| Triangular | 180 | 6 | 31.18 | 46.77 | 8.12 | −30.88 | 6.37 | 103,594 | 0.47 |
| Quadrilateral | 360 | 6 | 33.94 | 72.00 | 12.50 | −30.45 | 5.78 | 51,260 | 0.36 |
| Pentagonal | 540 | 6 | 35.27 | 85.60 | 14.86 | −32.62 | 5.43 | 66,340 | 0.33 |
| Hexagonal | 720 | 6 | 36.00 | 93.53 | 16.24 | −33.63 | 5.30 | 48,937 | 0.31 |
| Heptagonal | 900 | 6 | 36.45 | 98.51 | 17.10 | −33.58 | 5.18 | 56,371 | 0.30 |
| Octagonal | 1080 | 6 | 36.74 | 101.82 | 17.68 | −34.75 | 5.22 | 50,226 | 0.29 |
| Nonagonal | 1260 | 6 | 36.94 | 104.13 | 18.08 | −34.04 | 5.18 | 59,927 | 0.29 |
| Decagonal | 1440 | 6 | 37.08 | 105.80 | 18.37 | −33.57 | 5.10 | 44,621 | 0.29 |

## 4. Conclusions

In this investigation, we examine the performance of coplanar waveguide (CPW) structures loaded with split-ring resonators (SRRs) for microwave and RF applications. Our study reveals that the resonance frequency ($F_r$) of CPW-loaded SRR structures is influenced by the geometry of SRR shapes and the rotation angles of the gap, with certain shapes exhibiting enhanced performance characteristics. Linear regression analyses demonstrate correlations between polygonal SRR shapes and their transmission characteristics, underscoring the significance of structural geometry in dictating the electromagnetic response. Additionally, spectrogram analysis highlights symmetry and sensitivity to gap angle variations within the frequency range of 4 to 10 GHz, offering insights into the design and optimization of SRR-based devices for microwave engineering applications. This study found that the CPW-loaded triangular SRR structure is highly sensitive, exhibits the highest electric field distribution, and has the highest resonant frequency. Additionally, it possesses a spectrogram characteristic that differs from other structures. These findings contribute significant advances to the burgeoning field of CPW-loaded SRR structures, providing a robust framework for understanding their performance characteristics and paving the way for innovative advancements in microwave engineering and communication systems.

**Author Contributions:** Conceptualization, S.H.; methodology, S.H.; software, S.H. and S.S.; validation, S.H.; formal analysis, S.H.; investigation, S.H.; resources, S.H.; data curation, S.H.; writing—original draft preparation, S.H.; writing—review and editing, S.H.; visualization, S.H. and P.K.; supervision, S.H.; project administration, S.H.; funding acquisition, S.H. All authors have read and agreed to the published version of the manuscript.

**Funding:** This research project was financially supported by Mahasarakham University.

**Data Availability Statement:** The original contributions presented in this study are included in the article; further inquiries can be directed to the corresponding author.

**Conflicts of Interest:** The author declares no conflicts of interest.

## References

1. Pendry, J.B.; Holden, A.J.; Robbins, D.J.; Stewart, W.J. Magnetism from conductors and enhanced nonlinear phenomena. *IEEE Trans. Microw. Theory Tech.* **1999**, *47*, 2075–2084. [CrossRef]
2. Smith, D.R.; Padilla, W.J.; Vier, D.C.; Nemat-Nasser, S.C.; Schultz, S. Composite medium with simultaneously negative permeability and permittivity. *Phys. Rev. Lett.* **2000**, *84*, 4184–4187. [CrossRef] [PubMed]
3. Shelby, R.A.; Smith, D.R.; Schultz, S. Experimental verification of a negative index of refraction. *Science* **2001**, *292*, 77–79. [CrossRef] [PubMed]
4. Martín, F.; Falcone, F.; Bonache, J.; Marqués, R.; Sorolla, M. A new split ring resonator based left-handed coplanar waveguide. *Appl. Phys. Lett.* **2003**, *83*, 4652–4654. [CrossRef]
5. Falcone, F.; Martín, F.; Bonache, J.; Marqués, R.; Sorolla, M. Coplanar waveguide structures loaded with split-ring resonators. *Microw. Opt. Technol. Lett.* **2004**, *40*, 3–6. [CrossRef]
6. Falcone, F.; Lopetegi, T.; Baena, J.D.; Marques, R.; Martin, F.; Sorolla, M. Effective negative -ε stop-band microstrip lines based on complementary split ring resonators. *IEEE Microw. Wirel. Compon. Lett.* **2004**, *14*, 280–282. [CrossRef]
7. Baena, J.D.; Bonache, J.; Martin, F.; Marques, R.; Falcone, F.; Lopetegi, T.; Laso, M.A.G.; Garcia, J.; Gil, R.; Flores-Portillo, M.; et al. Equivalent circuit models for split-ring resonators and complementary split-ring resonators coupled to planar transmission lines. *IEEE Trans. Microw. Theory Tech.* **2005**, *53*, 1451–1461. [CrossRef]
8. Naqui, J.; Durán-Sindreu, M.; Martín, F. Novel sensors based on the symmetry properties of split ring resonators (SRRs). *Sensors* **2011**, *11*, 7545–7553. [CrossRef] [PubMed]
9. Naqui, J.; Duran-Sindreu, M.; Martin, F. Selective mode suppression in coplanar waveguide using metamaterial resonators. *Appl. Phys. A* **2012**, *109*, 1053–1058. [CrossRef]
10. Naqui, J.; Duran-Sindreu, M.; Martin, F. On the symmetry properties of coplanar waveguides loaded with symmetric resonators: Analysis and potential applications. In Proceedings of the IEEE/MTT-S International Microwave Symposium Digest, Montreal, QC, Canada, 17–22 June 2012; IEEE: Piscataway, NJ, USA, 2012.
11. Naqui, J.; Martin, F. Microwave sensors based on symmetry properties of resonator-loaded transmission lines. *J. Sens.* **2015**, *2015*, 741853. [CrossRef]
12. Naqui, J.; Martin, F. Transmission lines loaded with bisymmetric resonators and their application to angular displacement and velocity sensors. *IEEE Trans. Microw. Theory Tech.* **2013**, *16*, 4700–4713. [CrossRef]

13. Naqui, J.; Coromina, J.; Karami-Horestani, A.; Fumeaux, C.; Martin, F. Angular displacement and velocity sensors based on coplanar waveguides (CPWs) loaded with s-shaped split ring resonators (S-SRRs). *Sensors* **2015**, *15*, 9628–9650. [CrossRef] [PubMed]
14. Harnsoongnoen, S.; Charoen-In, U.; Pattitanang, S.; Auntarin, C.; Angkawisittpan, N. Angle sensor based on golden spiral–shaped tapered ring resonator using finite difference time-domain method. *Appl. Mech. Mater.* **2015**, *781*, 462–465. [CrossRef]
15. Horestani, A.K.; Duran-Sindreu, M.; Naqui, J.; Fumeaux, C.; Martin, F. Coplanar waveguides loaded with s-shaped split-ring resonators: Modeling and application to compact microwave filters. *IEEE Antennas Wirel. Propag. Lett.* **2014**, *13*, 1349–1352. [CrossRef]
16. Velez, P.; Naqui, J.; Duran-Sindreu, M.; Bonache, J.; Martin, F. Broadband microstrip bandpass filter based on open complementary split ring resonators. *Int. J. Antennas Propag.* **2012**, *2012*, 741853. [CrossRef]
17. Ebrahimi, A.; Withayachumnankul, W.; AlSarawi, S.F.; Abbott, D. Dual-mode behavior of the complementary electric-LC resonators loaded on transmission line: Analysis and applications. *J. Appl. Phys.* **2014**, *116*, 083705. [CrossRef]
18. Wu, B.; Liang, C.H.; Li, Q.; Qin, P.Y. Novel dual-band filter incorporating defected SIR and microstrip SIR. *IEEE Microw. Wirel. Compon. Lett.* **2008**, *18*, 392–394.
19. Herraiz-Martinez, F.J.; Garcia-Munoz, L.E.; Gonzalez-Ovejero, D.; González-Posadas, V.; Segovia-Vargas, D. Dual-frequency printed dipole loaded with split ring resonators. *IEEE Antennas Wirel. Propag. Lett.* **2009**, *8*, 137–140. [CrossRef]
20. Herraiz-Martinez, F.J.; Zamora, G.; Paredes, F.; Martin, F.; Bonache, J. Multiband printed monopole antennas loaded with open complementary split ring resonators for PANs and WLANs. *IEEE Antennas Wirel. Propag. Lett.* **2011**, *10*, 1528–1531. [CrossRef]
21. Herraiz-Martinez, F.J.; Paredes, F.; Zamora, G.; Martin, F.; Bonache, J. Dual-band printed dipole antenna loaded with open complementary split-ring resonators (OCSRRs) for wireless applications. *Microw. Opt. Technol. Lett.* **2012**, *54*, 1014–1017. [CrossRef]
22. Preradovic, S.; Balbin, I.; Karmakar, N.C.; Swiegers, G.F. Multiresonator-based chipless RFID system for low-cost item tracking. *IEEE Trans. Microw. Theory Tech.* **2009**, *57*, 1411–1419. [CrossRef]
23. Preradovic, S.; Chandra-Karmakar, N. Chipless RFID: Bar code of the future. *IEEE Microw. Mag.* **2010**, *11*, 87–98. [CrossRef]
24. Harnsoongnoen, S. Microwave sensors based on coplanar waveguide loaded with split ring resonators: A review. *Appl. Sci. Eng. Prog.* **2019**, *2*, 224–234. [CrossRef]
25. Naqui, J.; Duran-Sindreu, M.; Martin, F. Alignment and position sensors based on split ring resonators. *Sensors* **2012**, *12*, 11790–11797. [CrossRef]
26. Horestani, A.K.; Abbott, D.; Fumeaux, C. Rotation sensor based on horn-shaped split ring resonator. *IEEE Sens. J.* **2013**, *13*, 3014–3015. [CrossRef]
27. Horestani, A.K.; Fumeaux, C.; Al-Sarawi, S.F.; Abbott, D. Displacement sensor based on diamond-shaped tapered split ring resonator. *IEEE Sens. J.* **2013**, *13*, 1153–1160. [CrossRef]
28. Harnsoongnoen, S.; Wanthong, A. Real-time monitoring of sucrose, sorbitol, D-glucose and D-fructose concentration by electromagnetic sensing. *Food Chem.* **2017**, *232*, 566–570. [CrossRef] [PubMed]
29. Harnsoongnoen, S.; Wanthong, A. Coplanar waveguide transmission line loaded with electric LC resonator for determination of glucose concentration sensing. *IEEE Sens. J.* **2017**, *17*, 1635–1640. [CrossRef]
30. Harnsoongnoen, S.; Wanthong, A. Coplanar waveguides loaded with a split ring resonator-based microwave sensor for aqueous sucrose solutions. *Meas. Sci. Technol.* **2016**, *27*, 015103. [CrossRef]
31. Ebrahimi, A.; Withayachumnankul, W.; Al-Sarawi, S.; Abbott, D. High-sensitivity metamaterial-inspired sensor for microfluidic dielectric characterization. *IEEE Sens. J.* **2014**, *14*, 1345–1351. [CrossRef]
32. Ebrahimi, A.; Withayachumnankul, W.; AlSarawi, S.F.; Abbott, D. Metamaterial-inspired rotation sensor with wide dynamic range. *IEEE Sens. J.* **2014**, *14*, 2609–2614. [CrossRef]
33. Al-Naib, I.; Ateeq, I.S. Excitation of asymmetric resonance with symmetric split-ring resonator. *Materials* **2022**, *15*, 5921. [CrossRef] [PubMed]
34. Masrakin, K.; Ibrahim, S.Z.; Rahim, H.A.; Azemi, S.N.; Soh, P.J.; Tantiviwat, S. Microstrip sensor based on ring resonator coupled with double square split ring resonator for solid material permittivity characterization. *Micromachines* **2023**, *14*, 790. [CrossRef] [PubMed]
35. Zhao, Y.; Liu, Q.; Xu, Z.; Ji, G.; Mo, R. A split-ring resonator-loaded honeycomb sandwich structure for broadband microwave absorption. *Coatings* **2022**, *12*, 1706. [CrossRef]
36. Mosbah, S.; Zebiri, C.; Sayad, D.; Elfergani, I.; Bouknia, M.L.; Mekki, S.; Zegadi, R.; Palandoken, M.; Rodriguez, J.; Abd-Alhameed, R.A. Compact and highly sensitive bended microwave liquid sensor based on a metamaterial complementary split-ring resonator. *Appl. Sci.* **2022**, *12*, 2144. [CrossRef]
37. Kim, Y.; Park, E.; Salim, A.; Kim, J.; Lim, S. Microwave dual-crack sensor with a high Q-factor using the $TE_{20}$ resonance of a complementary split-ring resonator on a substrate-integrated waveguide. *Micromachines* **2023**, *14*, 578. [CrossRef] [PubMed]
38. Dahlberg, O.; Valerio, G.; Quevedo-Teruel, O. Fully metallic flat lens based on locally twist-symmetric array of complementary split-ring resonators. *Symmetry* **2019**, *11*, 581. [CrossRef]
39. Ren, K.; Zhu, P.; Sun, T.; Wang, J.; Wang, D.; Liu, J.; Zhao, W. A complementary split-ring resonator (CSRR)-based 2D displacement sensor. *Symmetry* **2022**, *14*, 1116. [CrossRef]

40. Abdulkarim, Y.I.; Özkan Alkurt, F.; Awl, H.N.; Altıntaş, O.; Muhammadsharif, F.F.; Appasani, B.; Bakır, M.; Karaaslan, M.; Taouzari, M.; Dong, J. A symmetrical terahertz triple-band metamaterial absorber using a four-capacitance loaded complementary circular split ring resonator and an ultra-thin ZnSe substrate. *Symmetry* **2022**, *14*, 1477. [CrossRef]
41. Vineetha, K.V.; Madhav, B.T.P.; Kumar, M.S.; Das, S.; Islam, T.; Alathbah, M. Development of compact bandpass filter using symmetrical metamaterial structures for GPS, ISM, Wi-MAX, and WLAN applications. *Symmetry* **2023**, *15*, 2058. [CrossRef]
42. Jameel, M.S.; Mezaal, Y.S.; Atilla, D.C. Miniaturized coplanar waveguide-fed UWB antenna for wireless applications. *Symmetry* **2023**, *15*, 633. [CrossRef]
43. Leo, A.; Bramanti, A.P.; Giusti, D.; Quaglia, F.; Maruccio, G. Reconfigurable split ring resonators by MEMS-driven geometrical tuning. *Sensors* **2023**, *23*, 1382. [CrossRef] [PubMed]
44. Zhan, Y.; Chen, Y.; Guo, H.; Wu, Q.; Li, M. Design of a Ka-band five-bit MEMS delay with a coplanar waveguide loaded U-shaped slit. *Micromachines* **2023**, *14*, 1508. [CrossRef] [PubMed]
45. Oh, Z.X.; Yeap, K.H.; Teh, P.C.; Dakulagi, V. Circular split-ring resonator-based sensor for dielectric constant measurement. *Microwave Opt. Technol. Lett.* **2023**, *65*, 513–518. [CrossRef]
46. Ong, C.S.; Yeap, K.H.; Chong, Z.L.; Nisar, H. An analysis of split-ring resonators and potential barcode application. *J. Eng. Technol. Appl. Phys.* **2024**, *6*, 76–81. [CrossRef]